ADVANCED FUNCTIONAL MATERIALS
www.afm-journal.de

Wearable Superhydrophobic Elastomer Skin with Switchable Wettability

Jian-Nan Wang, Yu-Qing Liu, Yong-Lai Zhang, Jing Feng, Huan Wang, Yan-Hao Yu, and Hong-Bo Sun**

Flexible smart surfaces with tunable wettability are promising for emerging wearable uses. However, currently, wearable superhydrophobic surfaces with dynamic wetting behaviors are rarely reported. Here, a skin-like superhydrophobic elastomer surface with switchable lotus leaf and rose petal states is reported. Direct laser writing technique is employed for one-step, programmable, large-scale fabrication of monolithic and hierarchical micro-nanostructures on elastomer, leading to strong water repellence. The surface topography can be finely regulated in a rapid and reversible manner by simple stretching, providing the feasibility of controlling the surface wettability by simple body motions. The ability to switch wetting states enables the surface to capture and release multiple droplets in parallel. Furthermore, the active surface can be applied to the joints of fingers and operate as a droplet manipulator under finger motions without requiring energy supply or external appliance. In this work, dynamic tuning of wetting properties is integrated into the design of skin-like wearable surfaces, revealing great potential in versatile applications such as wearable droplet manipulator, portable actuator, adaptive adhesion control, liquid repellent skin, and smart clothing.

1. Introduction

Mimicking natural intelligence provides a shortcut for engineers to devise advanced materials and capable systems.[1] Learning from nature always enables continued technical and scientific improvements. For example, innovative programmable biomaterials have been achieved based on DNA.[1c] Life-like systems have been synthesized by mimicking living cells.[1d] Biomineral-inspired materials morphology control have been performed at multiple scales.[1e] In the past decade, artificial water-repellent surfaces derived from superhydrophobic biointerfaces are of great value for a variety of applications such as self-cleaning,[2] antifreezing,[3] anticorrosion,[4] antibiofouling[5] and water/oil separation.[6] By mimicking different species, diverse artificial ultrahydrophobic surfaces that feature different wetting modes and functions have been successfully designed.[7,8] Especially, smart surfaces enabling reversible switching among distinct wetting states have attracted enormous research interests.[7,9–12] With the capability of reversible and dynamic wettability control, smart surfaces hold great potential for intelligent utilizations, such as rewritable devices,[10] adaptive materials,[11] and cell capture.[12] Beyond these well-developed applications, recently, devices equipped with superhydrophobic interfaces are also promising for emerging flexible and wearable uses.[13–15] For instance, Xiong et al. designed a wearable triboelectric generator based on water-proof textiles and realized energy harvesting from water.[13] Li et al. reported wearable electronics with salient superhydrophobic feature that facilitates the smooth run of devices under wet conditions,[14] the device life is thus potentially prolonged. Despite the aforementioned progresses, dewetting surfaces in wearable systems are usually attached merely as a protective layer. Wearable surfaces with dynamic wetting behavior, function like gecko skin[16] that features adaptive interface properties, are rarely reported. Combining active manipulation and multiple wetting properties with wearable applications is desirable not only to create advanced skin-compatible materials with intelligence and multifunction but also to explore novel utilizations of smart interface materials. A critical challenge is how to tailor the surface dewetting properties by mimicking real skin and to realize the controllable switching by simple stimulations.

Generally, wetting property is determined by surface energy and surface morphology. Hence, stimuli-responsive materials (SRMs) offer a superior choice for the design and engineering of smart surfaces, as they can alter their surface chemistry and/or topological structures under environmental stimuli (e.g., light, pH, heat, and solvents).[10,17–20] Although various tunable surfaces have been successively achieved, many reported regulating processes pose a potential risk to human health,

J.-N. Wang, Y.-Q. Liu, Prof. Y.-L. Zhang, Prof. J. Feng, Dr. H. Wang, Dr. Y.-H. Yu, Prof. H.-B. Sun
State Key Laboratory of Integrated Optoelectronics
College of Electronic Science and Engineering
Jilin University
2699 Qianjin Street, Changchun 130012, China
E-mail: yonglaizhang@jlu.edu.cn; hbsun@tsinghua.edu.cn
Dr. H. Wang, Prof. H.-B. Sun
State Key Laboratory of Precision Measurement Technology and Instruments
Department of Precision Instrument
Tsinghua University
Haidian, Beijing 100084, China
The ORCID identification number(s) for the author(s) of this article can be found under https://doi.org/10.1002/adfm.201800625.

DOI: 10.1002/adfm.201800625

such as the use of toxic and irritant chemicals, UV irradiation, and high temperature, which make them unfit for human-interactive applications. Besides, the long response time (e.g., minutes or hours) required in some processes to complete the state transition constitutes another barrier for practical implementation.

Recently, refined control of wettability has been successfully achieved using mild and chemical-free strategies. Wu et al. acquired switchable superhydrophobic states by controlling the curvature of a flexible film with micropillar-array structure.[21] Wong et al. demonstrated dynamic tuning of superhydrophobic states through strain-induced deformation of the nanofibers laid on an elastic substrate.[22] Huang et al. realized the switching between hydrophobic and hydrophilic via the expansion/contract of multiresponsive hydrogels decorated with salinized particles.[23] These pioneering works demonstrated the feasibility of tailoring wettability through mechanical reconfiguration. However, toward wearable usage, requirements including flexibility, on-demand switching, user-friendliness, and accessible actuation manners (e.g., simple body motions) have to be addressed, which constitutes another barrier hampering their practical applications.

Herein, we report a facile fabrication and potential wearable application of a smart superhydrophobic elastomer skin that can dynamically and reversibly switch between lotus leaf and rose petal modes by mimicking human skin structures. Direct laser writing (DLW) technique was employed to generate monolithic and hierarchical structures according to preprogrammed skin texture on elastomer substrate, which contributes to strong water repellence. Large-scale fabrication of skin-conformable surface with skin textures was demonstrated. The surface topography can be finely regulated in a rapid, reversible, and mild manner by simple body stretching, leading to an exquisite control of surface wettability at ambient condition with minimal damage to human body. The smart artificial skin can be applied to the joints of fingers to capture and release of droplets by finger motions without requiring energy supply or external appliance. The wearable smart skin would lead to versatile utilizations such as wearable manipulator, portable actuator, adaptive adhesion control, liquid repellent skin, and smart clothing.

2. Results and Discussion

2.1. Preparation of the Smart Surface

Considering the excellent flexibility and biocompatibility, polydimethylsiloxane (PDMS) elastomer widely used for electronic skin[24] and human motion monitoring[25] was employed as the base material. Laser manufacturing technology[26] featuring rapid, large-area, programmable, maskless prototyping was adopted for one-step surface microstructuring mimicking the characteristic skin textures (**Figure 1**a). Typically, a fingerprint-like and a hand palm-like surfaces with quasi-periodic irregular stripes (≈300–500 μm interval) were prepared that could be well compliant to the hand surface (Figure 1a and Figure S1, Supporting Information). Furthermore, the strategy could be extended to print diverse fingerprints (Figure 1b), large-scale pattern of a real hand size (Figure 1c), and hand back skin with irregular networks (Figure S1c, Supporting Information). As simplify, wearable surface (Figure 1d) could be designed with a uniform 400 μm period grating array (Figure 1e). Notably, magnified scanning electron microscopy (SEM) images (Figure 1f,g) revealed the simultaneous formation of a secondary micro/nanostructure. That arises from the violent laser-matter interaction during the laser ablation process. The ablation effect can be enhanced by increasing the laser power (2.8–3.6 W), and therefore nanostructures with increased density and tunable morphologies were readily obtained (Figure S2, Supporting Information). In this work, structures fabricated at 3.6 W were selected as the optimal design because the widely distributed microscale papillae covered with nanospikes (Figure 1g) finely resembles the characteristic surface textures of lotus leaves.[27] The facile laser processing endowed the surface with a monolithic and hierarchical structure, while the elastomer permitted a rapid and reversible deformation capability, both of which guaranteed a valid tailoring of surface geography in micro- and nanoscale under external force without fear of delamination.

2.2. Strain-Modulated Structures and Wettability

By tuning the strength and direction of the applied strain, the surface structure can be regulated in a controllable manner. We recorded the morphologies and profiles of the structure at different strain values using confocal laser scanning microscopy (CLSM). The strain value (ε) is defined by the film length at the tensile state (L) and the initial state (L_0) according to the equation $\varepsilon = (L - L_0)/L_0$. Especially, as the structure was designed to be anisotropic, distinct driving modes were obtained with strain directions perpendicular (**Figure 2**) and parallel (**Figure 3**) to the grating orientation. Exertion of the perpendicular stretching led to a controlled expansion of the gratings with an increased period and a decreased height (Figure 2c). In contrast, the parallel strain forced the texture to compress and gave rise to the decreases of period and height (Figure 3c). The ability to flexibly adjust surface features (e.g., structural parameters) is expected to enable continuous tuning of wettability between a set of wetting states at different strain values.

To assess the wetting behaviors under tensile control, we monitored the variation of contact angles (CAs, θ) and sliding angles (SAs, α) in directions parallel (||) and perpendicular ($\perp$) to the grating orientation, respectively, as static and dynamic characterizations. Considering the multiscale micro/nanostructures and the hydrophobic nature of PDMS polymer (CA = 111.0°), the prepared surface is promising for strong water repellence without extra low-surface-energy treatment (e.g., self-assembly or chemical grafting of fluorine molecules) which was commonly required to enhance material hydrophobicity. As proved by the measurements, the relaxed surface ($\varepsilon = 0$) exhibited high CAs in excess of 150° ($\theta_\perp = 155.04°$, $\theta_\parallel = 152.52°$) and small SAs lower than 10° ($\alpha_\perp = 3.5°$, $\alpha_\parallel = 2.5°$), indicating its superhydrophobicity. In the pursuit of compatibility with human and environment, there is a trend to develop fluorine-free strategy. This facile strategy provides an approach for green production of antiwater surfaces. Subjected to the above-mentioned two distinct reconfiguration modes, the surface was found to exhibit totally different wetting performances.

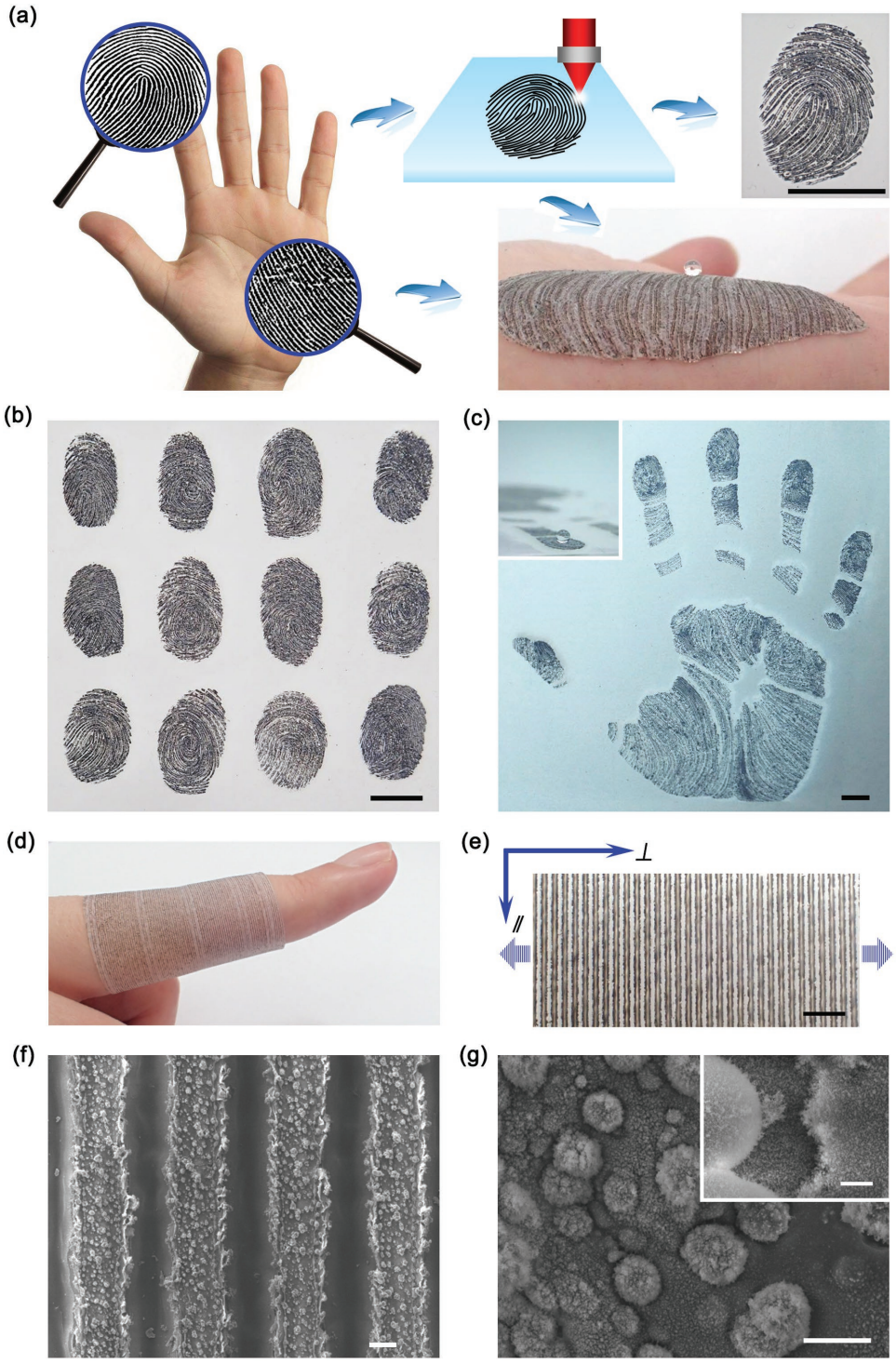

Figure 1. a) Schematic illustration of the manufacture of skin-like wearable surface by DLW technique. b) Laser-printed diverse fingerprints. c) Liquid repellent palm of a real hand size. d) Wearable structured surface with e) periodic gratings. f,g) SEM images of the hierarchical structures of the gratings. Scale bars: a–c) 1 cm, e) 1.6 mm, f) 100 µm, g) 10 µm, (inset) 5 µm.

Figure 4a,b shows the relationship of CA and SA with respect to the level of perpendicular strains, respectively. As the stress increased, a clear transformation of wetting states was demonstrated. When $\varepsilon < 50\%$, water droplet on the surface exhibited a spherical shape and readily rolled off with a slight tilt (Figure 4b, left inset), we call it "rolling state." The superior water repellency resulted in high CAs and low SAs in both directions ($\theta > 150°$, $\alpha < 10°$). When the strain increased to a larger value ($\varepsilon > 70\%$), although there was a slight decrease in CA ($\theta_{\perp} > 150°$, $\theta_{\parallel} < 145°$), the sample was still highly hydrophobic, making the droplet

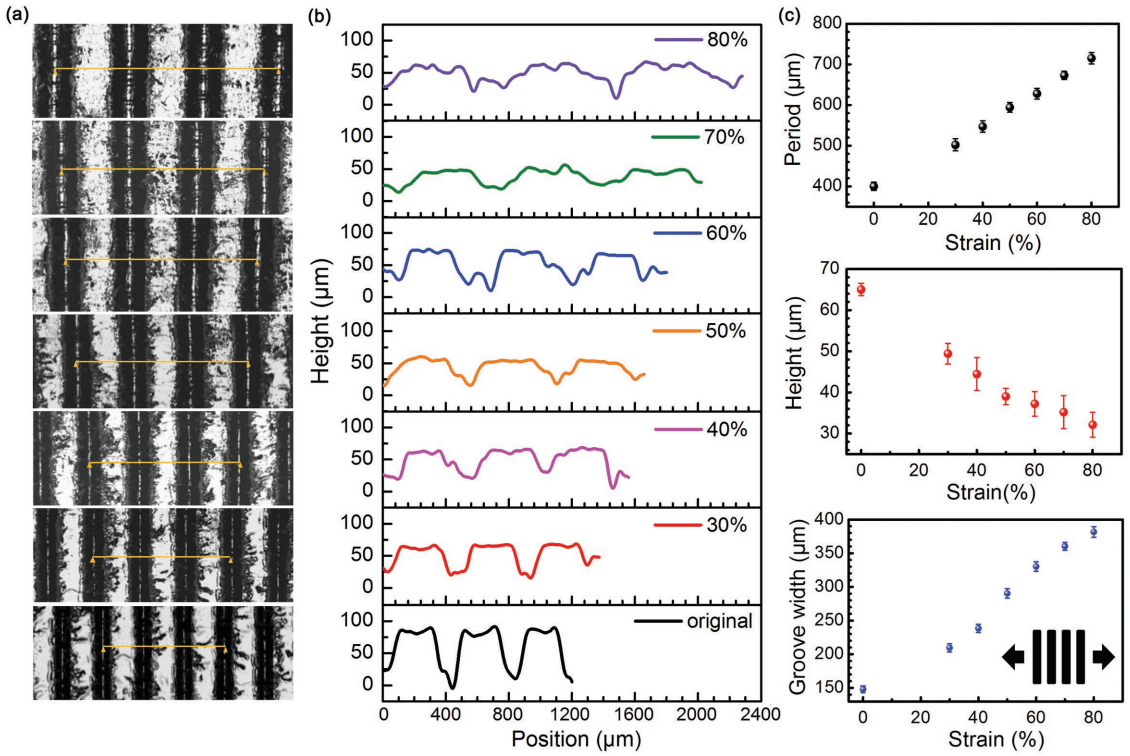

Figure 2. Variation of the a) morphology, b) profile, and c) structural parameters under applied strains perpendicular to the grating orientation.

standing on the sample intact. In contrast, it could not move freely but firmly stuck on the sample even in a reversed state ($\alpha = 180°$) (Figure 4b, right inset), we refer it to "pinning state."

To evaluate the feasibility of dynamic wettability regulation, the switching process was monitored in real time (Figure S3 and Video S1, Supporting Information). The sample was first highly

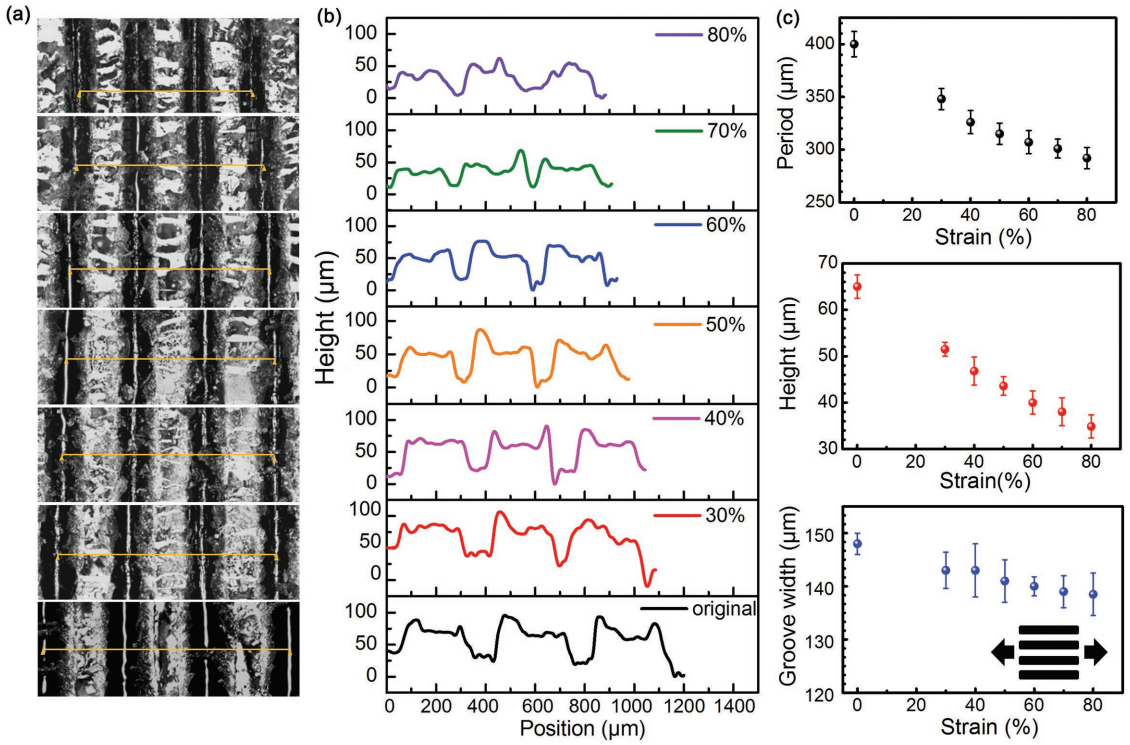

Figure 3. Variation of the a) morphology, b) profile, and c) structural parameters under applied strains parallel to the grating orientation.

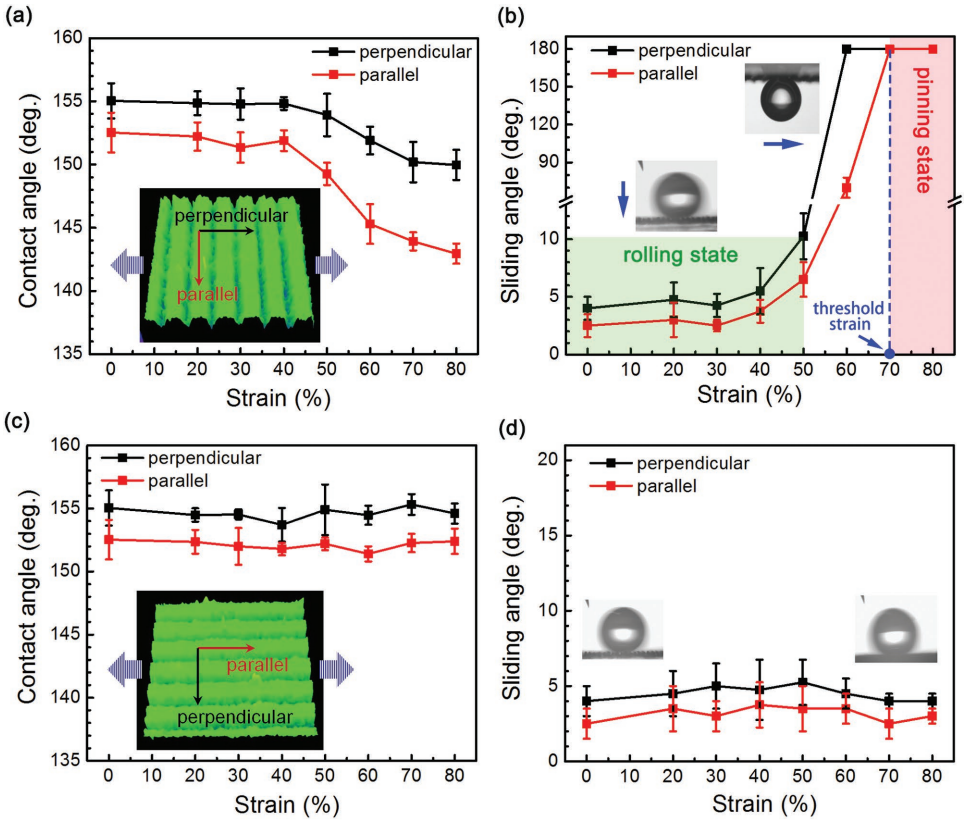

Figure 4. a) CAs and b) SAs of the surface in two directions as a function of the perpendicular strain values. There is a wetting transition from rolling to pinning states. c) CAs and d) SAs of the surface as a function of the parallel strain values. The surface presented durable superhydrophobicity in rolling state.

stretched ($\varepsilon = 80\%$), seven droplets (≈5 µL) were randomly added at different locations. Then the surface was erected (90° tilted), all of the droplets were still adhered on it without affected by the gravitation. Upon relaxation, all of the droplets instantaneously fell off leaving the surface empty and dry, confirming an in situ and high speed alteration of wetting modes.

As another driving strategy, the surface was pulled in parallel direction. In contrast, the exhibited rolling ultraphobicity was found to be mechanically robust. The sample kept almost stable CAs (Figure 4c) and SAs independent of the strain levels (Figure 4d). We gradually increased the strains from 20% to 80%, droplets were hard to stay on the strained surface (5° tilted) no matter where they encountered the sample (Figure S4 and Video S2, Supporting Information).

According to the above results, switchable superhydrophobicity can be achieved by tuning the direction and strength of the exerted force. Cyclic tests further demonstrated the reversibility of the dynamic switching (**Figure 5**a). Moreover, the switching performance can be modified by rationally modulating the grating parameters. By programmable DLW technique, a series of grating arrays with periods ranging from 300 to 500 µm were prepared (laser power 3.6 W) (Figure S5, Supporting Information). We characterized the threshold strain (Figure 4b) for state transition to evaluate the efficiency of wettability switching. Within the elastic limit, sensitive mechanical regulation with low critical strain value is desirable. As shown in Figure 5b, a mild threshold value (48%) is accessible with a larger period.

2.3. Mechanism of the Wettability Switching

Within the elastic limit, the resilient reconfiguration can be attributed to the directional elongation of the molecular chain along the strain direction. In this regard, mechanical stress that can induce elongation, isomerization, disentanglement, and cleavage of molecules may alter material properties, accordingly.[28] To investigate the influence of these chemical features on the mechanical wettability tuning, we characterized water CA of a flat PDMS slice (without structure) at different strain value (Figure S6a, Supporting Information). Providing that the flat elastomer in the relaxed and stretching states possess similar surface roughness, the wettability changes can be ascribed to the mechanical stretching induced molecular conformation changes. The test results showed that conformational changes can alter the surface wettability slightly.

To get further insight into the transition mechanism, we observed the water/solid interfaces and investigated the contact modes at the two contrasting states. At rolling state (e.g., ε = 0%), droplet took on a spherical shape, having a small contact area with the underlying surface (**Figure 6**a). Optical microscopic (OM) image (Figure 6b) revealed that the contact region was wholly wrapped by bright coating, indicating the presence of air which further decreased the actual solid/liquid contact area dramatically. The air layer and pocket act as water shield, preventing droplet from wetting the grating top and penetrating into the groove bottom. That is why droplet seemed to be lifted by the

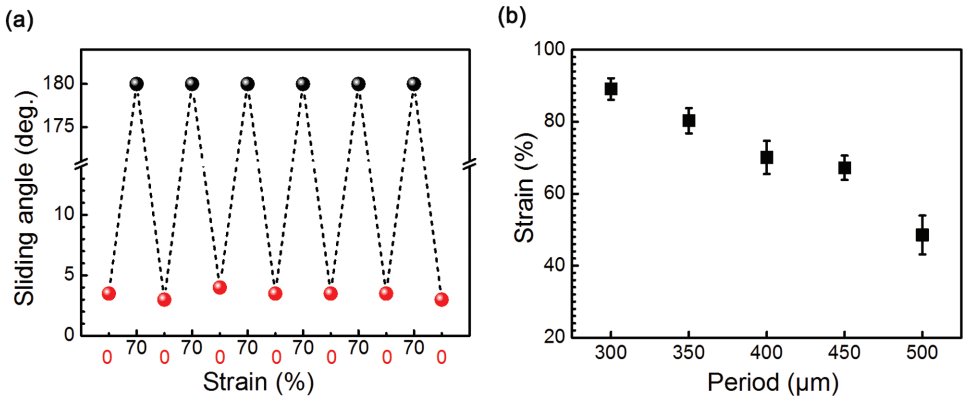

Figure 5. a) Reversible switching between rolling and pinning states under cyclic strains. b) Dependence of the threshold strain on the grating period.

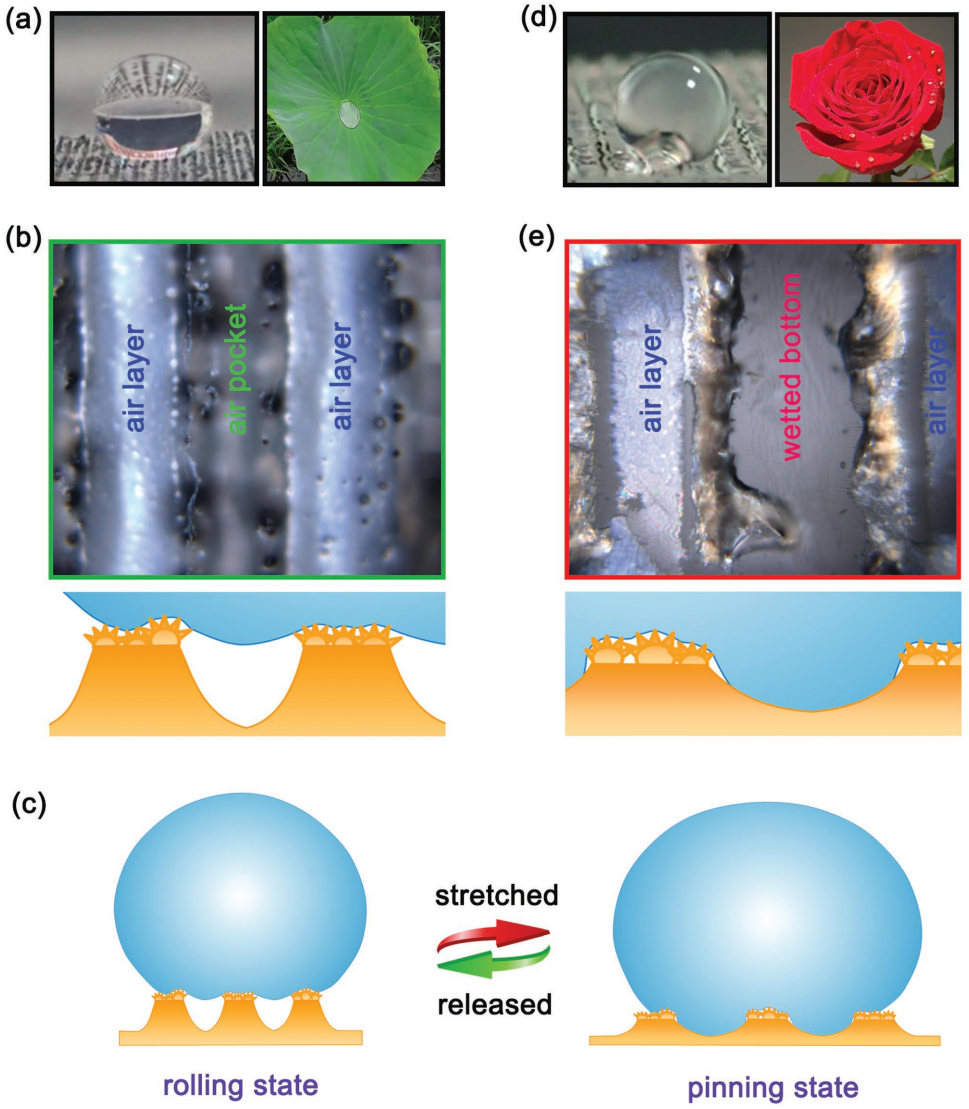

Figure 6. a) Photograph of a water droplet on the surface in the rolling state ($\varepsilon = 0\%$) and b) OM image of the liquid/solid interface. c) Schematic illustration of the wetting models. d) Photograph of a water droplet on the surface in the pinning state ($\varepsilon = 70\%$) and e) OM image of the liquid/solid interface.

surface (Figure 6a) and could roll off effortlessly, mimicking "lotus effect." The contact mode is thus illustrated as shown in Figure 6c, in compliance with Cassie–Baxter's model.[29] While for pinning state (e.g., ε = 70%), the limited solid/surface contact region (Figure 6d) was partially wetted according to the enlarged detail (Figure 6e). The grating top was still protected by air. However, the previously observed bright pocket in the bottom disappeared, indicating the infiltration of droplet. That can be attributed to the formation of wider and lower groove during structural reconfiguration (Figure 2c), which promoted the immersion. The intimate water-solid contact generated strong interaction and resulted in sticky superhydrophobicity (Figure 6d), resembling "petal effect."[30] Figure 6c illustrates the pinning model accordingly. These results indicated that the transition from Cassie's to Wenzel's mode[31] occurred as the strain reached a critical level and enabled wettability switching.

In addition to pure water, strong repellency for coffee, tea, milk, sugar, and NaCl solutions was also demonstrated as shown in Figure S6b in the Supporting Information. And the mechanical wettability switching can be generalized to these liquids. While for organic solvents such as ethanol, acetone, and hexane, the surface was completely wetted. To achieve broader applicability of this concept to these oil liquids, refined structural design needs to be addressed such as the introduction of re-entrant texture.[7]

2.4. Wearable Droplet Manipulator

To test the feasibility of combining dynamic wettability tuning with wearable application, several aspects were considered. (1) The smart surface is nontoxic, and stretching/bending manipulation is user-friendly, so that the surface is compatible with human-interactive uses. (2) The flexible surface can conform to the shape of clothing or human body. (3) The threshold strain (50–70%) is achievable for body movement, therefore the dynamic surface can be manipulated by human themselves independent of energy supply or external appliance. As demonstrated previously (Video S2, Supporting Information), the ability to adjust wetting states allowed the uniform smart surface to maneuver multiple droplets in parallel. We further applied the active surface to the joint of an index finger and presented a miniaturized droplet tweezer (Video S3, Supporting Information). The on/off switching could be controlled by bending or unbending the finger (**Figure 7**a). The object droplet was first placed on a superhydrophobic substrate. Upon contact with the stretched surface, the droplet was carefully seized due to the pinning effect. Keeping the bending gesture allowed the flexible transport of the droplet to the target location, where we could be on-demand release it by stretching the finger to trigger the rolling state. In this way, surface microfluidic technology, which is vital for biochemical analysis and clinical diagnostics, was simply imparted to a "tweezer on finger" by integrating rose-petal-like and lotus-leaf-like dewetting properties into a wearable surface.

3. Conclusion

In conclusion, a smart elastomer skin capable of switching between pinning and rolling superhydrophobic states was conveniently fabricated, simply manipulated, and utilized for wearable droplet handling. DLW technique was employed to create programmable skin-like microtextures and tunable nanostructures on elastomer in one step, which contributes to extreme hydrophobicity, excellent skin conformability, and reversible deformation capabilities. Mechanical stretching enabled a rapid, continuous, and reversible control over surface topography and wettability in a user-friendly manner. The acceptable strain value (50–70%) for wettability switching was promising for practical applications. As a typical example, the smart skin could be attached to movable joints and complete tweezer-like mission to

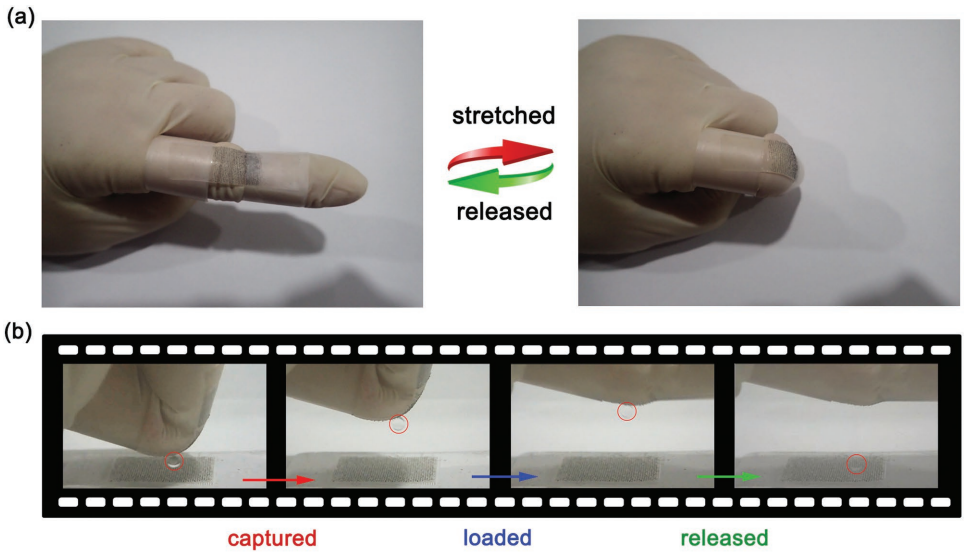

Figure 7. a) Exertion and release of a strain on the wearable surface by human motions. b) "Tweezer on finger" demonstrating capture, transfer, and release of a water droplet.

realize controllable capture and release of droplet by bending or stretching fingers. Our results provide new insights to develop smart wearable surfaces with multifunction and intelligence. Moreover, it has been proven that mechanical modulation of surface features is valuable for the development of smart windows,[32] stretchable organic light-emitting devices (OLEDs),[33] wearable sensing electronics.[14] Taking advantage of the superhydrophobicity-induced fascinating properties such as antifogging, drag reduction and ice-proofing,[7] wearable surfaces with mechano-modulated dewetting properties would be promising for a wide range of applications.

4. Experimental Section

Materials and Laser Fabrication: The deformable surface was prepared using PDMS elastomer comprising base polymer and curing agent (Sylgard 184 Silicone Elastomer kit, Dow Corning Corporation, USA). They were mixed together (10:1 by weight) and cured at 85 °C for 1 h. Programmable patterns including skin-like textures and periodic gratings with different periods (300–500 μm) were generated on the surface using a carbon dioxide laser engraving machine (JW6090, JG., China) with different laser powers (2.8–3.6 W). Different tensile stains (20–80%) were exerted on the surface using a home-made strain stage.

Characterization: SEM images were obtained by using a field-emission scanning microscope (JSM-7500F, JEOL, Japan). The CA tests were performed using a contact angle meter (SL200B, Solon Tech., China). Confocal laser scanning microscopy images were obtained using an LEXT 3D measuring laser microscope (OLS4100, Olympus, Japan).

Supporting Information

Supporting Information is available from the Wiley Online Library or from the author.

Acknowledgements

The authors acknowledge the National Key Research and Development Program of China and National Natural Science Foundation of China under Grants #2017YFB1104300, #61522503, #61590930, #61775078, and #61605055 for support. Consent was obtained from the human subject in the respective experiments.

Conflict of Interest

The authors declare no conflict of interest.

Keywords

biomimetic smart surfaces, laser processing, stretchable skins, switchable superhydrophobicity, wearable applications

Received: January 24, 2018
Revised: February 28, 2018
Published online: April 6, 2018

[1] a) C. Zhang, D. A. Mcadams, J. C. Grunlan, *Adv. Mater.* **2016**, *28*, 6292; b) C. Sanchez, H. Arribart, M. M. G. Guille, *Nat. Mater.* **2005**, *4*, 277; c) G. N. Pandian, H. Sugiyama, *Bull. Chem. Soc. Jpn.* **2016**, *89*, 843; d) B. C. Buddingh, J. C. M. van Hest, *Acc. Chem. Res.* **2017**, *50*, 769; e) Y. Oaki, *Bull. Chem. Soc. Jpn.* **2017**, *90*, 776.
[2] Y. Lu, S. Sathasivam, J. Song, C. R. Crick, C. J. Carmalt, I. P. Parkin, *Science* **2015**, *347*, 1132.
[3] L. Wang, Q. Gong, S. Zhan, L. Jiang, Y. Zheng, *Adv. Mater.* **2016**, *28*, 7729.
[4] D. Zang, R. Zhu, W. Zhang, X. Yu, L. Lin, X. Guo, M. Liu, L. Jiang, *Adv. Funct. Mater.* **2017**, *27*, 1605446.
[5] P. Zhang, L. Lin, D. Zang, X. Guo, M. Liu, *Small* **2017**, *13*, 1503334.
[6] F. Chen, Y. Lu, X. Liu, J. Song, G. He, M. K. Tiwari, C. J. Carmalt, I. P. Parkin, *Adv. Funct. Mater.* **2017**, *27*, 1702926.
[7] S. Wang, K. Liu, X. Yao, L. Jiang, *Chem. Rev.* **2015**, *115*, 8230.
[8] K. Liu, L. Jiang, *Nano Today* **2011**, *6*, 155.
[9] Y. Huang, B. B. Stogin, N. Sun, J. Wang, S. Yang, T. S. Wong, *Adv. Mater.* **2017**, *29*, 1604641.
[10] T. Lv, Z. Cheng, D. Zhang, E. Zhang, Q. Zhao, Y. Liu, L. Jiang, *ACS Nano* **2016**, *10*, 9379.
[11] X. Yao, Y. Hu, A. Grinthal, T. S. Wong, L. Mahadevan, J. Aizenberg, *Nat. Mater.* **2013**, *12*, 529.
[12] S. Hou, H. Zhao, L. Zhao, Q. Shen, K. S. Wei, D. Y. Suh, A. Nakao, M. A. Garcia, M. Song, T. Lee, B. Xiong, S. C. Luo, H. R. Tseng, H. H. Yu, *Adv. Mater.* **2013**, *25*, 1547.
[13] J. Xiong, M. F. Lin, J. Wang, S. L. Gaw, K. Parida, P. S. Lee, *Adv. Energy Mater.* **2017**, *7*, 1701243.
[14] L. Li, Y. Bai, L. Li, S. Wang, T. Zhang, *Adv. Mater.* **2017**, *29*, 1702517.
[15] J. E. Mates, I. S. Bayer, J. M. Palumbo, P. J. Carroll, C. M. Megaridis, *Nat. Commun.* **2015**, *6*, 8874.
[16] L. F. Boesel, C. Greiner, E. Arzt, A. del Campo, *Adv. Mater.* **2010**, *22*, 2125.
[17] Y. Liu, X. Wang, B. Fei, H. Hu, C. Lai, J. H. Xin, *Adv. Funct. Mater.* **2015**, *25*, 5047.
[18] Z. Xu, Y. Zhao, H. Wang, H. Zhou, C. Qin, X. Wang, T. Lin, *ACS Appl. Mater. Interfaces* **2016**, *8*, 5661.
[19] Z. L. Wu, A. Buguin, H. Yang, J. M. Taulemesse, N. Le Moigne, A. Bergeret, X. Wang, P. Keller, *Adv. Funct. Mater.* **2013**, *23*, 3070.
[20] X. Wang, G. Qing, L. Jiang, H. Fuchs, T. Sun, *Chem. Commun.* **2009**, 2658.
[21] D. Wu, S. Z. Wu, Q. D. Chen, Y. L. Zhang, J. Yao, X. Yao, L. G. Niu, J. N. Wang, L. Jiang, H. B. Sun, *Adv. Mater.* **2011**, *23*, 545.
[22] W. S. Y. Wong, P. Gutruf, S. Sriram, M. Bhaskaran, Z. Wang, A. Tricoli, *Adv. Funct. Mater.* **2016**, *26*, 399.
[23] X. Huang, Y. Sun, S. Soh, *Adv. Mater.* **2015**, *27*, 4062.
[24] H. H. Chou, A. Nguyen, A. Chortos, J. W. F. To, C. Lu, J. Mei, T. Kurosawa, W. G. Bae, J. B. H. Tok, Z. Bao, *Nat. Commun.* **2015**, *6*, 8011.
[25] a) Y. R. Jeong, J. Kim, Z. Xie, Y. Xue, S. M. Won, G. Lee, S. W. Jin, S. Y. Hong, X. Feng, Y. Huang, J. A. Rogers, J. S. Ha, *NPG Asia Mater.* **2017**, *9*, e443; b) Y. Cao, H. Ota, E. W. Schaler, K. Chen, A. Zhao, W. Gao, H. M. Fahad, Y. Leng, A. Zheng, F. Xiong, C. Zhang, L. C. Tai, P. Zhao, R. S. Fearing, A. Javey, *Adv. Mater.* **2017**, *29*, 1701985.
[26] M. Malinauskas, A. Zukauskas, S. Hasegawa, Y. Hayasaki, V. Mizeikis, R. Buividas, S. Juodkazis, *Light: Sci. Appl.* **2016**, *5*, e16133.
[27] L. Feng, S. Li, Y. Li, H. Li, L. Zhang, J. Zhai, Y. Song, B. Liu, L. Jiang, D. Zhu, *Adv. Mater.* **2002**, *14*, 1857.
[28] a) K. Ariga, K. Minami, M. Ebara, J. Nakanishi, *Polym. J.* **2016**, *48*, 371; b) K. Ariga, T. Mori, J. P. Hill, *Adv. Mater.* **2012**, *24*, 158.
[29] A. B. D. Cassie, S. Baxter, *Trans. Faraday Soc.* **1944**, *40*, 546.
[30] L. Feng, Y. Zhang, J. Xi, Y. Zhu, N. Wang, F. Xia, L. Jiang, *Langmuir* **2008**, *24*, 4114.
[31] R. N. Wenzel, *Ind. Eng. Chem.* **1936**, *28*, 988.
[32] S. G. Lee, D. Y. Lee, H. S. Lim, D. H. Lee, S. Lee, K. Cho, *Adv. Mater.* **2010**, *22*, 5013.
[33] D. Yin, J. Feng, R. Ma, Y. F. Liu, Y. L. Zhang, X. L. Zhang, Y. G. Bi, Q. D. Chen, H. B. Sun, *Nat. Commun.* **2016**, *7*, 11573.